




Article

# Multibeam Cylindrical Conformal Array in the Presence of Enhanced Mutual Coupling

Xianyang Lv <sup>1,2</sup>, Yongwei Zhang <sup>1,\*</sup>, Quan Shi <sup>1,\*</sup>, Yanwei Fu <sup>1</sup>, Murat Temiz <sup>1,3</sup>, Ahmed El-Makadema <sup>4</sup> and Hongliang Li <sup>1</sup>

<sup>1</sup> School of Transportation and Civil Engineering, Nantong University, Nantong 226019, China; lvxianyang@ntu.edu.cn (X.L.); yanwei\_fu@stmail.ntu.edu.cn (Y.F.); m.temiz@ucl.ac.uk (M.T.); lhliang@ntu.edu.cn (H.L.)

<sup>2</sup> School of Information Science and Technology, Nantong University, Nantong 226019, China

<sup>3</sup> Department of Electronic and Electrical Engineering, University College London, London WC1E 7JE, UK

<sup>4</sup> Department of Electrical and Electronic Engineering, The University of Manchester, Manchester M13 9PL, UK; ahmed\_makadema@manchester.ac.uk

\* Correspondence: david.y.zhang@ntu.edu.cn (Y.Z.); sq@ntu.edu.cn (Q.S.)

**Abstract:** The limitations of conventional sensors have made array antennas increasingly crucial for gathering information and communication applications in intelligent transportation and communication systems. Compact cylindrical arrays are particularly favored for their ability to achieve azimuth angle scanning. However, the substantial mutual coupling effect between the elements on curved surfaces and its implication for these arrays remain unclear, which is a key factor to consider when such arrays are used for multibeam applications. This study investigates the effect of mutual coupling in a dual-slant-polarized cylindrical array. The results showed that mutual coupling is predominantly observed among the closely located elements, and it is essential for achieving an ultra-wide bandwidth. The study also analyzes the impact of mutual coupling on the scan impedance and radiation characteristics for multibeam applications and reveals that these arrays exhibit robust multibeam capability, hence having great potential for use in sensing and communication applications.

**Keywords:** conformal array; cylindrical array; dual-polarization; mutual coupling



**Citation:** Lv, X.; Zhang, Y.; Shi, Q.; Fu, Y.; Temiz, M.; El-Makadema, A.; Li, H. Multibeam Cylindrical Conformal Array in the Presence of Enhanced Mutual Coupling. *Electronics* **2024**, *13*, 373. <https://doi.org/10.3390/electronics13020373>

Academic Editor: David A. Sánchez-Hernández

Received: 14 November 2023

Revised: 7 January 2024

Accepted: 11 January 2024

Published: 16 January 2024



**Copyright:** © 2024 by the authors. Licensee MDPI, Basel, Switzerland. This article is an open access article distributed under the terms and conditions of the Creative Commons Attribution (CC BY) license (<https://creativecommons.org/licenses/by/4.0/>).

## 1. Introduction

Modern communication and sensing technologies such as remote sensing (RS) or 5G and next-generation communications heavily rely on antenna arrays to maximize spectral efficiency and system performance. For instance, RS is a technology embedded in interdisciplinary sciences, which aims to gather information and analyze objects without making any kind of physical contact. Its idea had its origin in topographic mapping of the Earth's surface when the camera was first invented. The technology has flourished in many sectors in addition to its original purpose of surface mapping mainly related to geography. For instance, one widely known instrument based on this technology is the Geographic Information System (GIS) [1–3]. The application of RS technologies has been increasingly seen in transportation systems and vehicles due to the growing developments in assisted and autonomous driving technologies [4]. RS sensors for data collection [5,6] have witnessed tremendous developments in recent years.

RS sensors measure the properties of electromagnetic (EM) radiation reflected from an object's surface. Technology for developing microwave sensors is quite different from that of optical-infrared (OIR) sensors [7]. Sensors based on microwaves have two advantages: data about specific geographic locations can be gathered despite weather conditions, and the targets' parameters related to polarization can be acquired.

The ability of RS sensors to provide accurate and reliable data on weather and road surface conditions was investigated in [8]. These conventional sensors based on infrared

radiation or spectroscopic methods have shown a limited distance coverage (i.e., up to 15 m), and the accuracy is heavily dependent on various conditions. Future intelligent transportation systems (ITSs) will need to collect various information about the surroundings of the vehicle regardless of weather conditions in order to improve mobility, transport safety, and comfort while also reducing the negative impacts on the environment. Phased arrays with multi-dimensional electronic scanning capability have advantages for ITSs [9,10] and RS systems [11]. Transportation systems can be improved with the use of the data uncovered by wireless sensing in combination with high data rate wireless communications. Moreover, recently, dual-function systems have been proposed to combine sensing and communications on the same platform for vehicular networks further to improve both energy efficiency and system performance [12].

The primary sensing technologies for ITS are summarized and compared in Table 1, which demonstrates that sensing with EM waves, such as in integrated communication and sensing systems, provides high accuracy and significant advantages over other methods in complex environments. Low-cost and compact antenna arrays and beamforming technologies are necessary in modern vehicular systems to provide high-accuracy sensing and high data rate communications.

**Table 1.** Primary sensing technologies for ITSs and RS systems.

| Sensing Technology               | Principle of Operation                      | Disadvantages   | Advantages  |
|----------------------------------|---|---|---|
| Cameras [13,14]                  | Image analysis                              | Affected by heavy rain, fog, sun and other bad weather, by the interference of light.   | High horizontal resolution; can recognize lane lines, speed limit signs, and other traffic information, as well as pedestrians. |
| Acoustic sensors [15,16]         | Acoustic pressure measurement               | Complex computations are necessary to eliminate impact of other sound sources.  | Robust against light and weather variations; monitoring of multiple traffic lanes is possible.                                  |
| LIDARs [17,18]                   | Detection of reflected electromagnetic wave | The recognition of objects depends on the characteristics of objects in the database; difficult to identify lane lines. The distance ranging and speed measurement accuracy are low. Optical devices are easily polluted. | High resolution; sensitive response speed; not easily affected by ambient light; can recognize the contour of the object.       |
| Light sensors [19,20]            | Light intensity measurement.                | Sensitive to light and weather variations. Cleaning is necessary.   | Monitoring of multiple traffic lanes is possible. Enables pedestrian and bicycle detection. Detection range is wide,            |
| Passive infrared sensors [21,22] | Infrared radiation measurement              | Does not have the ability of angle detection; cannot complete stationary ranging; ranging is short and vulnerable to bad weather.   | Can accurately identify organisms; low cost; can work at night.   |
| Ultrasonic sensors [23,24]       | Detection of reflected sound waves          | The angle cannot be identified; the detection range is short; the Doppler effect is obvious; the reliability is poor.   | The hardware structure is simple; the cost is low; short distance measurement of high resolution.                               |

Table 1. Cont.

| Sensing Technology                        | Principle of Operation                  | Disadvantages   | Advantages   |
|---|---|---|--|
| Integrated communication and sensing [12] | Measurement of received signal strength | Disturbed by road objects greatly; cannot recognize lane lines and road sign.                           | Strong anti-interference ability, high spatial resolution, long detection range, high reliability. Works 24/7; can work in bad weather conditions. |
| Millimeter-wave automotive radar [25–28]  | Measurement of frequency and waveform   | Range and susceptibility to adverse weather conditions; complexity of signal processing; limited range. | Accurate distance measurement with shorter wavelength; improved object detection; high resolution; reduced interference.                           |

The antenna or elements generally behave very differently when they are isolated or located in an array. The impedance, radiation pattern, and efficiency of the antennas in an array are dominated by the mutual coupling with the neighboring elements. The spacing between the elements and the geometry of the array influence the mutual coupling [29]. Mutual coupling may be utilized to increase the bandwidth of the antenna arrays [30]. The characteristics of mutual coupling in an array are complex, particularly for non-planar arrays, for instance, cylindrical conformal arrays. Therefore, it is important to study and understand mutual coupling and its benefits and disadvantages in non-planar arrays, especially in the case of multibeam applications.

Unlike a planar antenna array, a cylindrical conformal array (CCA) can provide omnidirectional coverage around the antenna array [30–32]. This feature is especially desired for scientific applications, for example, Cylindrical Polarimetric Phased Array Radar (CPPAR) is capable of maintaining broadside polarimetric purity at all azimuthal directions [33]. The angular measurement errors of differential reflectivity on the order of 0.1 dB were expected for polarimetric weather radar missions. This is a substantial challenge to achieve for planar arrays due to azimuth scan losses and the significant polarization bias that occurs when the main lobe is steered away from the principal planes [34]. The sidelobe level in the cylindrical array is investigated and controlled by selecting the appropriate angular variation of the noise amplitude [35]. The arrays on a cylinder can be analyzed by employing Bessel functions to obtain solutions for active element patterns and mutual coupling relationship between elements, which is typically represented by an impedance matrix [36–38].

As the technology for ITSs is developed, the demand for the coverage of both a wider range and a broader spectrum increases. In addition, polarimetric measurement with a high polarization purity is critical to improve classification accuracy in certain conditions. The dual slant-polarized cylindrical array based on the tightly coupled crossed disk antennas is known to provide a high polarization purity.

In this study, an ultrawideband cylindrical array based on tightly coupled crossed disk elements was investigated. The potential of such arrays for forming multiple beams is explored by considering the subarrays of various sizes. The contributions of the paper are as follows: (1) It shows that the enhanced coupling made a positive contribution to improving impedance matching and radiation efficiency of the array; (2) It reveals that mutual coupling in the cylindrical array is more concentrated in a local area on the array aperture than in the counterpart planar array; (3) The characteristic of the mutual coupling distribution in a cylindrical array of crossed disks is unique and has advantages over other forms of arrays to produce multiple beams with a low profile in structure.

The remainder of this paper is organized as follows, in Section 2, the dual slant-polarized cylindrical array for a study on the mutual coupling effect is described. Section 3 analyzes the effect of mutual coupling with respect to impedance matching and radiation characteristics. The results and discussion are presented in Section 4, and finally, a conclusion is drawn in Section 5.

### 2. Theory of Cylindrical Arrays

When two or more antennas are placed close to each other, an interchange of energy occurs. This happens whether the antennas are in transmitting or receiving mode. The energy exchange between the antenna elements in the array is caused by mutual coupling. The mutual coupling changes the terminal impedance, antenna gain, beamwidth, and efficiency of the array. In order to investigate this effect more thoroughly on a cylindrical surface with a more-complex element structure, a dipole array as shown in Figure 1 was examined first. The mutual coupling between the element “1” with a length  $l$  and the surrounding elements with a side-by-side configuration is expressed by [39]

$$R_{41} = \frac{\eta}{4\pi} [2C_i(u_0) - C_i(u_1) - C_i(u_2)], \tag{1}$$

$$X_{41} = -\frac{\eta}{4\pi} [2S_i(u_0) - S_i(u_1) - S_i(u_2)], \tag{2}$$

$$u_0 = kd$$

$$u_1 = k(\sqrt{d^2 + l^2} + l) \tag{3}$$

$$u_2 = k(\sqrt{d^2 + l^2} - l)$$

where  $S_i(x)$  and  $C_i(x)$  are the sine and cosine integral functions and  $d$  is the distance between the two dipoles of interest at the feed point.

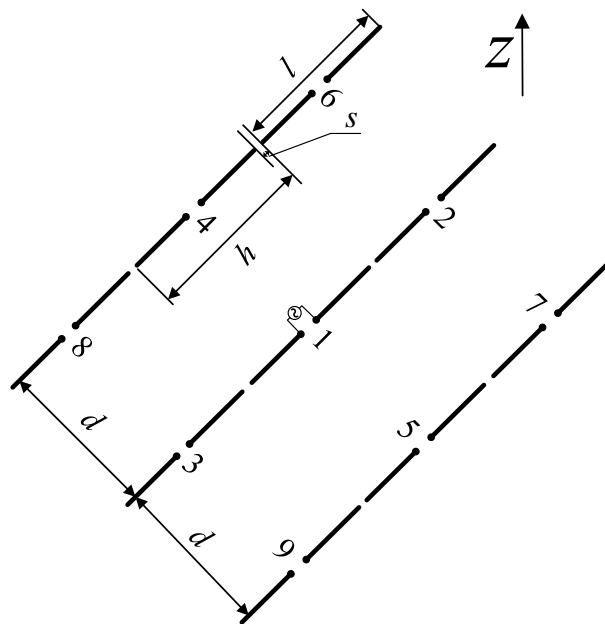


Figure 1. Scan impedance analysis of the array consisting of 9 half-wavelength dipoles.

For the collinear configuration, the mutual impedance is expressed by

$$R_{21} = -\frac{\eta}{8\pi} \cos(v_0) [-2C_i(2v_0) + C_i(v_2) + C_i(v_1) - \ln(v_3)] + \frac{\eta}{8\pi} \sin(v_0) [2S_i(2v_0) - S_i(v_2) - S_i(v_1)] \tag{4}$$

$$X_{21} = -\frac{\eta}{8\pi} \cos(v_0) [2S_i(2v_0) - S_i(v_2) - S_i(v_1)] + \frac{\eta}{8\pi} \sin(v_0) [2C_i(2v_0) - C_i(v_2) - C_i(v_1) - \ln(v_3)] \tag{5}$$

$$\begin{aligned}
v_0 &= kh \\
v_1 &= 2k(h+l) \\
v_2 &= 2k(h-l) \\
v_3 &= (h^2 - l^2)/h^2
\end{aligned} \tag{6}$$

For the parallel-in-echelon configuration, the mutual impedance is expressed by

$$\begin{aligned}
R_{61} &= -\frac{\eta}{8\pi} \cos(w_0) [-2C_i(w_1) - 2C_i(w_1') + C_i(w_2) \\
&\quad + C_i(w_2') + C_i(w_3) + C_i(w_3')] \\
&\quad + \frac{\eta}{8\pi} \sin(w_0) [2S_i(w_1) - 2S_i(w_1') - S_i(w_2) \\
&\quad + S_i(w_2') - S_i(w_3) + S_i(w_3')]
\end{aligned} \tag{7}$$

$$\begin{aligned}
X_{61} &= -\frac{\eta}{8\pi} \cos(w_0) [2S_i(w_1) + 2S_i(w_1') - S_i(w_2) \\
&\quad - S_i(w_2') - S_i(w_3) - S_i(w_3')] \\
&\quad + \frac{\eta}{8\pi} \sin(w_0) [2C_i(w_1) - 2C_i(w_1') - C_i(w_2) \\
&\quad + C_i(w_2') - C_i(w_3) + C_i(w_3')]
\end{aligned} \tag{8}$$

$$\begin{aligned}
w_0 &= kh \\
w_1 &= k(\sqrt{d^2 + h^2} + h) \\
w_1' &= k(\sqrt{d^2 + h^2} - h) \\
w_2 &= k(\sqrt{d^2 + (h-l)^2} + (h-l)) \\
w_2' &= k(\sqrt{d^2 + (h-l)^2} - (h-l)) \\
w_3 &= k(\sqrt{d^2 + (h+l)^2} + (h+l)) \\
w_3' &= k(\sqrt{d^2 + (h+l)^2} - (h+l))
\end{aligned} \tag{9}$$

The total antenna efficiency is used to take into account losses at the input terminals and within the structure of the antenna. The total efficiency of the elements in the array is related to the impedance matching status, partially dependent on the mutual coupling effect. The total efficiency and the active input impedance of the element have the following relationship:

$$\Gamma = \frac{Z_{in} - Z_0}{Z_{in} + Z_0} \tag{10}$$

where  $\Gamma$  is the voltage reflection coefficient at the input terminals of the antenna,  $Z_{in}$  is antenna input impedance, and  $Z_0$  is the characteristic impedance of the transmission line.

$$e_r = 1 - |\Gamma|^2 \tag{11}$$

where  $e_r$  is reflection efficiency.

$$e_0 = e_r e_c e_d \tag{12}$$

where  $e_0$  is the total antenna efficiency,  $e_c$  is the conduction efficiency, and  $e_d$  is the dielectric efficiency.

$$e_0 = e_r e_{cd} = e_{cd} (1 - |\Gamma|^2) \tag{13}$$

where  $e_{cd} = e_c e_d$  is the antenna radiation efficiency [40]. It is usually implicit to compute and measure; however, it can be obtained from full-wave simulations with high accuracy, and it was adopted in this investigation.

The calculated terminal impedance, mutual coupling coefficients, active input impedance, and total radiation efficiency of the element “1” in the presence of the eight other elements are given in Table 2. This indicates that, as the number of active elements increases, the real part fluctuates around the characteristic value, and the absolute value of the imaginary part of the input impedance tends to decrease; hence, the total radiation efficiency of the center element also tends to decrease. The total radiation efficiency reaches 99% with all nine elements becoming active. However, the operational bandwidth of such arrays is limited. Hence, mutually coupled disk arrays were designed and studied; furthermore, they were put on a curved surface for a low profile and accommodating the array carriers of uneven surfaces; the unique features of such arrays were investigated based on disk arrays with enhanced mutual coupling.

**Table 2.** The active input impedance of the center element in the dipole array.

| Element No. | $Z_{11}$     | $Z_{21}/Z_{31}$ | $Z_{41}/Z_{51}$   | $Z_{61}/Z_{71}/Z_{81}/Z_{91}$ | $Z_1$             | Total Efficiency in dB (%) |
|-------------|--------------|-----------------|-------------------|-------------------------------|-------------------|----------------------------|
| 1           | $73 + j42.5$ | NA              | NA                | NA                            | $73 + j42.5$      | −0.6444 (86.21)            |
| 3           | $73 + j42.5$ | $26.5 + j19.6$  | NA                | NA                            | $126 + j81.7$     | −1.7437 (66.93)            |
| 5           | $73 + j42.5$ | $26.5 + j19.6$  | $-12.53 - j29.93$ | NA                            | $100.94 + j21.84$ | −0.6154 (86.79)            |
| 9           | $73 + j42.5$ | $26.5 + j19.6$  | $-12.53 - j29.93$ | $-11.89 - j7.85$              | $53.38 - j9.56$   | −0.0416 (99.05)            |

The designed array formed by mutually coupled disk pairs demonstrated broad bandwidth characteristics. It is also bendable to make it deployable on curved surfaces. This array structure was chosen for studying the mutual coupling effect because coupling in this arrangement is essential for the array to obtain broad bandwidth. The cylindrical array is in a dual slant-polarized configuration, and mutual coupling between the elements was significant to yield a low profile. The wideband cylindrical array design is shown in Figure 2. It consists of three layers: one active layer of tightly coupled crossed disks in the middle and one metasurface on the outside, backed up by a ground plane in the core of the cylinder with a smaller radius and hole inside. These three layers are concentric. Four subarray configurations are also illustrated where 1, 3, 5, or 9 elements are included in the subarray, respectively. The cross-section view of the cylindrical array is shown in Figure 3.

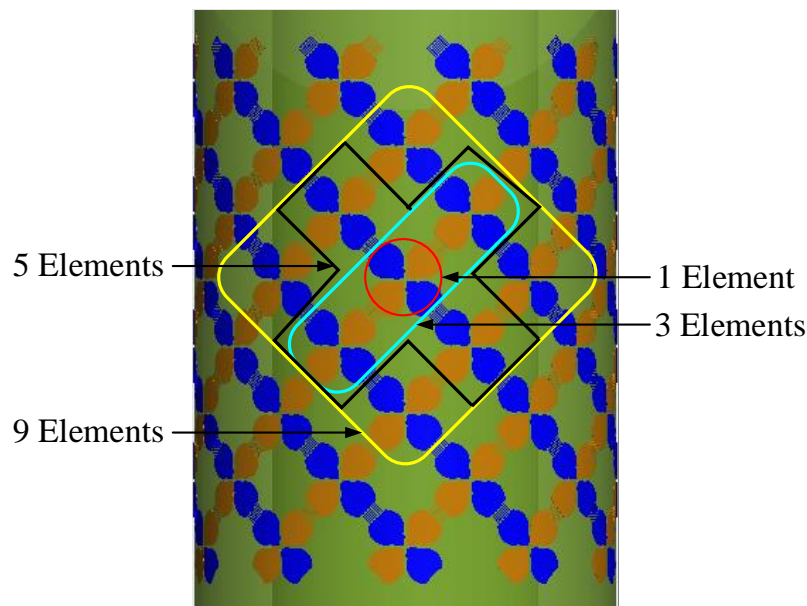


**Figure 2.** The subarrays consisting of 1, 3, 5, or 9 elements are separately excited to investigate beam-forming performance. Blue and orange element colours indicate the two orthogonal polarizations.



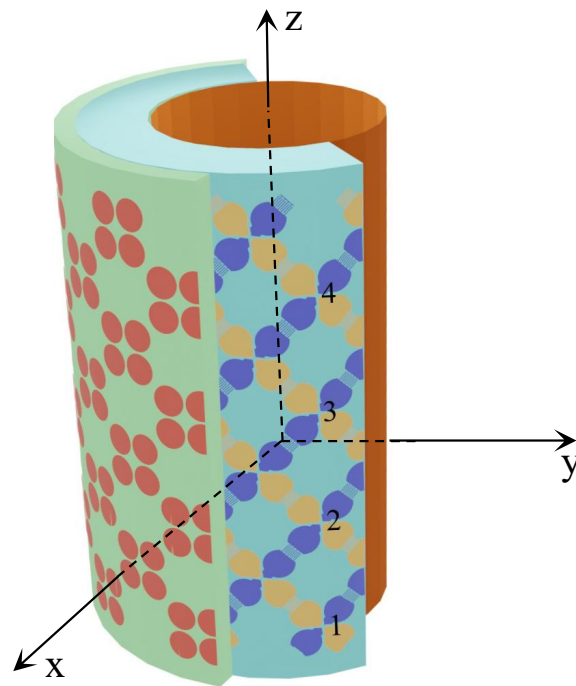


**Figure 3.** View of the cylindrical array of tightly coupled crossed disks antennas, where “1”, “2”, “3”, and “4” refer to the four dual-polarized (blue and orange) elements in a column.

### 3. The Method for Analysis

The effect of mutual coupling on impedance matching and radiation characteristics of the elements in a cylindrical array has been examined in this study. The mutual coupling between the center element and its surrounding elements in the cylindrical array and its corresponding reference planar array are illustrated in Figure 4 for comparison, where (3,3) represents the physical location of the center element. The element in the center with 4 other adjacent elements (two at each side in  $+45^\circ$ , i.e., the orientation for co-polarization) formed the center row of the  $5 \times 5$  subarray. Three frequencies of 3 GHz, 4 GHz, and 5.9 GHz were studied for the element in the two forms of the array.

It is clearly shown in Figure 4 that mutual coupling between the elements in a planar array is spreading over a greater electrical distance than the same elements in a cylindrical form. In other words, the mutual coupling effect in a cylindrical array can be observed only between a few surrounding elements rather than being observed across the  $5 \times 5$  subarray. This implies that a small subarray (with  $3 \times 3$  elements in it) of the cylindrical array can demonstrate the potential benefits of the entire array, in particular the operation frequency bandwidth. This unique feature enables the cylindrical array to form agile multiple beams with a relatively low profile. It was also noticed that the center element has a stronger coupling with the elements in the same row-collinear position than the elements in the parallel rows. Hence, irregular subarrays can be formed with more elements in the center row to improve its radiation performance. Three aspects of array characteristics have been investigated, including impedance matching, far-field radiation patterns, and multibeam scan capability. They are all closely related to the mutual coupling effect, with each having a different role in planar arrays being compared and analyzed.

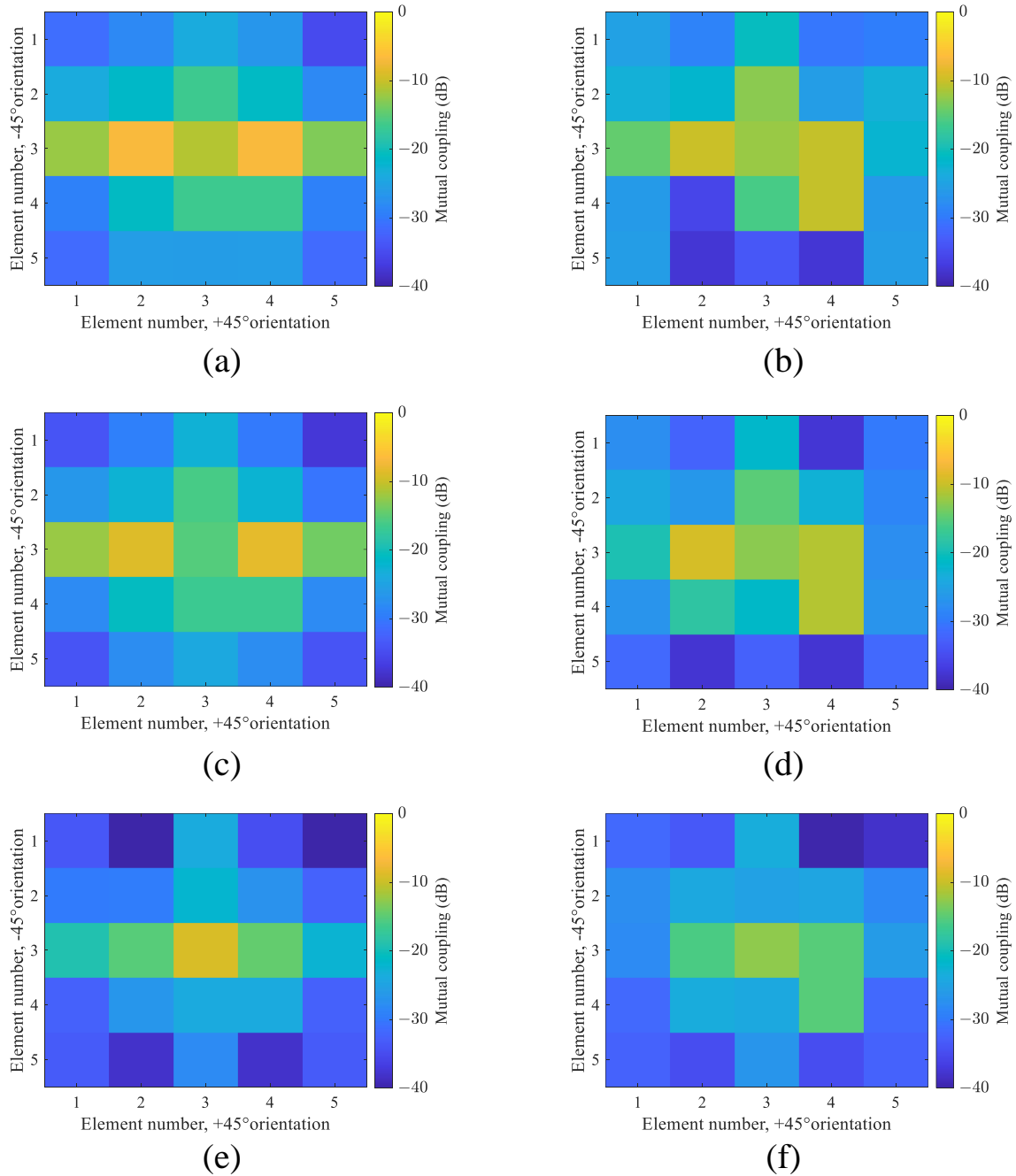


**Figure 4.** Comparison of mutual coupling between the center element and surrounding elements in the cylindrical array and the reference planar array at different frequencies. (a) Planar array at 3 GHz; (b) cylindrical array at 3 GHz; (c) planar array at 4 GHz ; (d) cylindrical array at 4 GHz; (e) planar array—5.9 GHz; (f) cylindrical array at 5.9 GHz. The mutual coupling between the elements in the cylindrical array is based on the tightly coupled crossed disk elements.

In a cylindrical array, the mutual impedance  $Z_{nm}$  between the element  $n$  and the element  $m$  in the paraxial region can be calculated in closed form by analyzing the surface tangential field at the position of the  $m$ th element excited by a hypothetical current source (with the current mode,  $\mathbf{J}_n$ ) representing the element  $n$ ; it is simply given by [41,42]

$$Z_{nm} = \int_{S_m} \mathbf{E}_n \cdot \mathbf{J}_n ds \quad (14)$$



where  $\mathbf{E}_n$  is the field due to the source  $\mathbf{J}_n$  and  $S_m$  is the area occupied by the source  $\mathbf{J}_m$ . The current modes were assumed to be sinusoidal current sources (with an infinitesimal length, approximately  $0.05\lambda_0$ ) along the polarized direction of the element. Relation between  $\mathbf{E}_n$  and  $\mathbf{J}_n$  can be represented by a dyadic Green's function. As the tangential components of the dyadic Green's function are periodic, hence, it can be approximated by a Fourier series (FS). The oscillatory nature of the coupling as the separation changes indicated that there are at least two types of field contributions adding in and out of phase. This characteristic is demonstrated in Table 2 and Figure 4, where, for a fixed separation between two elements, mutual coupling changes with frequency in a periodic manner.

### 3.1. Effect on Impedance Matching

The active reflection coefficient for the element  $m$  at a scan angle  $(\theta_0, \varphi_0)$  for a finite array has the following relation with the scattering parameters [40]:

$$\Gamma_{act,m}(\theta_0, \varphi_0) = \sum_{n=1}^N S_{m,n} e^{-jk(x_n \sin\theta_0 \cos\varphi_0 + y_n \sin\theta_0 \sin\varphi_0)} \quad (15)$$

where  $(x_n, y_n)$  is the position of the element  $n$ ,  $k$  is the wavenumber,  $S_{m,n}$  is the scattering parameter demonstrating mutual coupling between two elements of  $m$  and  $n$ , and  $N$  is the total number of elements in the array for observation.

Figure 5 shows the active reflection coefficient of the center elements (the elements "2" and "3" shown in Figure 3) in the cylindrical array, compared with the active reflection coefficient of the unit cell for the reference planar array at the broadside scan. This indicates that, with fewer elements in the cylindrical array configuration, the array elements can work collaboratively over a broad frequency bandwidth, and more active elements are needed in the case of a planar array.

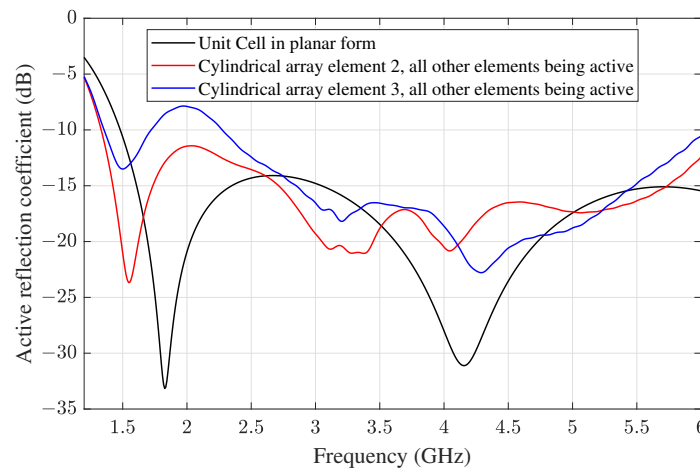


**Figure 5.** The active reflection coefficients of the center elements "2" and "3" in the cylindrical array, compared with the active reflection coefficient of the unit cell in an infinite reference planar array.

Figure 6 shows the active reflection coefficient of the center element in the subarrays consisting of 1, 3, 5, and 9 elements, respectively. This clearly indicates that, as the number of active element in the subarrays increases, the input impedance becomes more matched; the active reflection coefficient is lower and better. The operational band of the antenna array covered the frequency range from 1.7 GHz to 6 GHz. The efficiency, reflection coefficients and input impedance at 1.7 GHz, 2.5 GHz, 4 GHz, and 5.9 GHz with 1, 3, 5, and 9 elements in the subarrays are presented in Table 3.

**Table 3.** The input impedance of the center element and total efficiency of the subarrays.

| Frequency | Number of Mutual Coupling Elements | S-Parameters dB | $Z_{in}$<br>$\Omega$ | Total Antenna Efficiency<br>dB (%) |
|-----------|------------------------------------|-----------------|----------------------|------------------------------------|
| 1.7 GHz   | 1                                  | −3.9486         | 62.82 − j130.66      | −2.2391 (59.72)                    |
|           | 3                                  | −3.9204         | 27.76 − j24.12       | −2.2583 (59.45)                    |
|           | 5                                  | −8.0147         | 53.00 − j16.81       | −0.7466 (84.20)                    |
|           | 9                                  | −30.1146        | 116.16 − j6.29       | −0.0042 (99.90)                    |
| 2.5 GHz   | 1                                  | −8.3272         | 77.3413 − j67.655    | −0.6904 (85.30)                    |
|           | 3                                  | −7.8620         | 76.310 + j72.498     | −0.7759 (83.64)                    |
|           | 5                                  | −17.0512        | 140.95 + j30.367     | −0.0865 (98.03)                    |
|           | 9                                  | −17.0527        | 139.46 − j31.102     | −0.0865 (98.03)                    |
| 4 GHz     | 1                                  | −14.5749        | 95.351 − j32.346     | −0.1542 (96.51)                    |
|           | 3                                  | −5.8523         | 362.52 − j47.795     | −1.3070 (74.01)                    |
|           | 5                                  | −11.7313        | 194.92 − j33.444     | −0.3018 (93.29)                    |
|           | 9                                  | −14.1703        | 161.27 − j37.123     | −0.1695 (96.17)                    |
| 5.9 GHz   | 1                                  | −12.4752        | 81.31 + j29.03       | −0.2528 (94.34)                    |
|           | 3                                  | −13.8363        | 91.36 − j32.73       | −0.1834 (95.87)                    |
|           | 5                                  | −16.3371        | 99.60 − j26.86       | −0.1021 (97.68)                    |
|           | 9                                  | −16.9269        | 91.5265 + j9.96      | −0.0890 (97.97)                    |

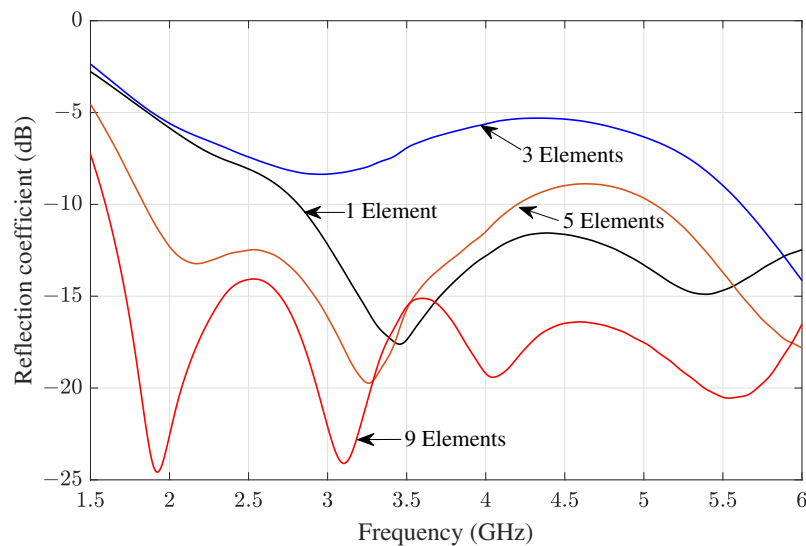


**Figure 6.** The active reflection coefficient for the subarrays consisting of a different number of active elements, where 1, 3, 5, or 9 elements became active simultaneously. The center element of the subarrays was observed in all scenarios.

### 3.2. Effect on the Radiation Pattern

The active element pattern of the array is considered when a single element is excited when all other array elements are terminated with matched loads. In this case, the radiation pattern of the array is significantly affected by the position of the element that is excited. Moreover, all mutual coupling effects also influence the radiation pattern.

The array beam pattern is calculated by [43]

$$F(\theta) = EP \cdot AF, \tag{16}$$

where the array factor (*AF*) describes the spatial response of all array elements. For the element pattern (*EP*), unlike the traditional element pattern in a planar array, the normal of each array element is oriented in a different direction in a conformal array. The element pattern can be defined by [43]

$$EP(\theta, \phi) = \hat{\mathbf{n}}_i, \hat{\mathbf{r}}, \tag{17}$$

where

$$\hat{\mathbf{n}}_i = \frac{\mathbf{r}_i}{|\mathbf{r}_i|}, \quad (18)$$

where  $\hat{\mathbf{r}}$  is the spatial unit vector and  $\hat{\mathbf{n}}_i$  is the normal vector for the  $i$ th element position.

The radiation patterns of the subarrays consisting of different numbers of elements were investigated. The patterns were synthesized under two different scenarios: (1) the radiation patterns of the subarrays were generated while all the other elements in the cylindrical array were terminated with matched loads; (2) the radiation patterns of the subarrays were produced while all the rest elements were left open.

The radiation patterns for four subarray scenarios on the cylindrical surfaces are compared in Figure 7. The number of elements in the subarrays was 1, 3, 5, and 9 respectively, and the radiation patterns of the four frequencies are given. As expected, as the number of elements in the subarray increases, the beamwidth becomes narrower. The pattern in the  $XOY$ -plane is narrower than in the  $YOZ$ -plane, which reflects the dipole-like nature of such antenna elements. The characteristics of the radiation patterns of subarrays are summarized in Table 4, where the intermediate frequency of 4 GHz was selected. As expected, the 3 dB beamwidth becomes gradually narrower in both planes as the number of active elements increases. The scenario with three elements in the subarray shows a slightly odd feature compared to other cases; this may be due to poor impedance matching, as shown in Figure 6.

The total efficiencies of the subarrays formed by different numbers of elements are shown in Figure 8. The trend is clear that the total efficiency of the subarrays increases with the total number of active elements in the subarrays. This is in particular more obvious at a low frequency, where mutual coupling between the adjacent elements plays a more-significant role in improving impedance matching and, accordingly, the efficiency. However, there is an exception in certain frequencies such as at 4 GHz, where a degraded performance for the subarray with three elements is observed compared to that of a single active element; this is due to the phenomenon that the negative mutual coupling effect occurs, making the impedance matching worse. The deteriorated impedance matching from a single element to a subarray with three elements is shown in Figure 6.

### 3.3. Multibeam Capabilities

As shown in Figure 4, a significant coupling concentrated among only a few close elements is a unique characteristic of the cylindrical array based on the tightly coupled disk antennas. This feature can be adapted to produce multiple beams by forming many subarrays on the cylindrical surface. The number of beams the array can produce depends on the impedance matching of the elements in the subarray, the total number of elements, the dimension of the array, and the beam characteristic required.

It was demonstrated that a subarray with nine elements on the cylindrical surface yields the best impedance matching for the center elements of the four subarrays studied. In the cylindrical array with 80 elements (dual-polarized), as shown in Figure 3, 10 beams were formed by establishing 10 subarrays; they were distributed uniformly in the horizontal plane. The radiation patterns of the 10 subarrays (of nine elements in each subarray) are shown in Figure 9. The characteristics of the radiation beams for the subarrays of different sizes at 2.5 GHz are summarized in Table 4. For the subarray with a size of  $3 \times 3$ , a gain of 10.54 dB can be obtained from each subarray, and 10 subarrays on the cylindrical surface can cover the entire horizontal space. The 3 dB beamwidth in the elevation plane is broader than  $40^\circ$ . The realized gains of all subarrays showed little discrepancy among them. Azimuth-scan-invariant beam characteristics are demonstrated.

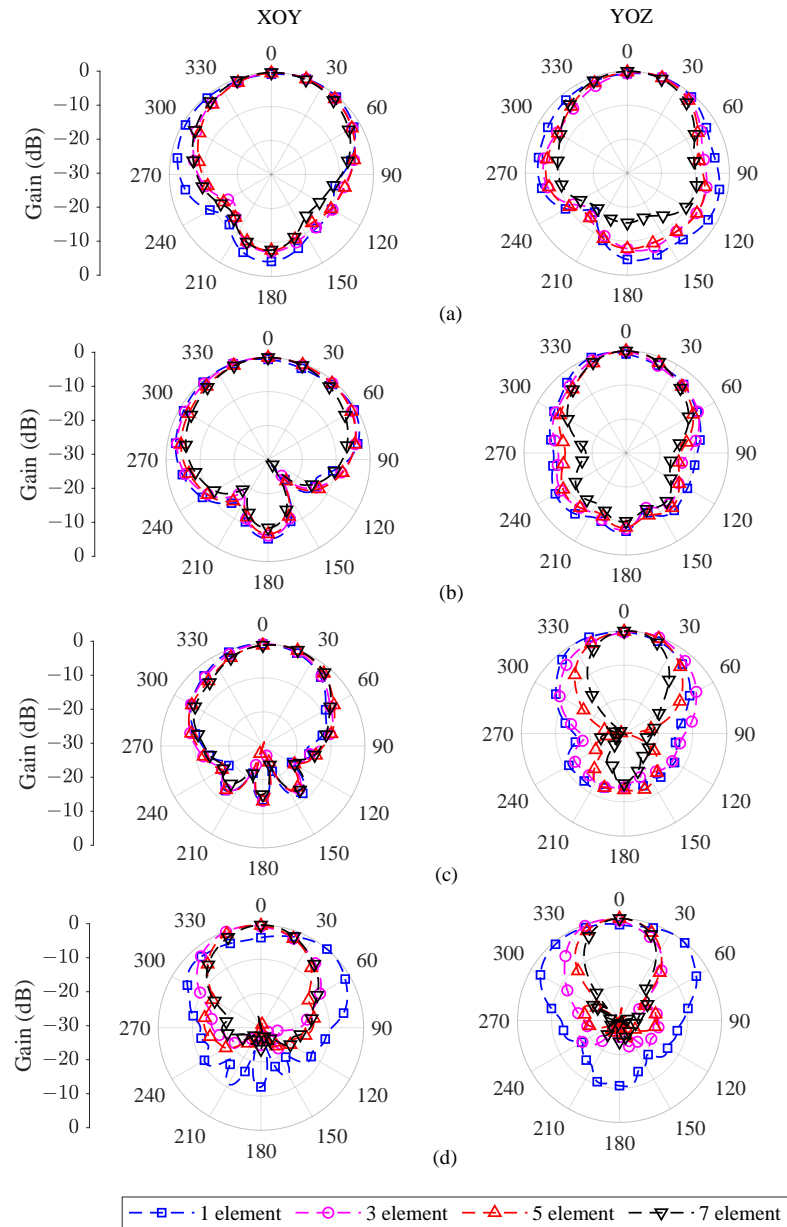


**Figure 7.** Simulated radiation patterns of 4 subarray scenarios on the cylindrical surfaces; a subarray with 1, 3, 5, or 9 elements was excited, respectively: (a) 1.7 GHz, (b) 2.5 GHz, (c) 4 GHz, and (d) 5.9 GHz.

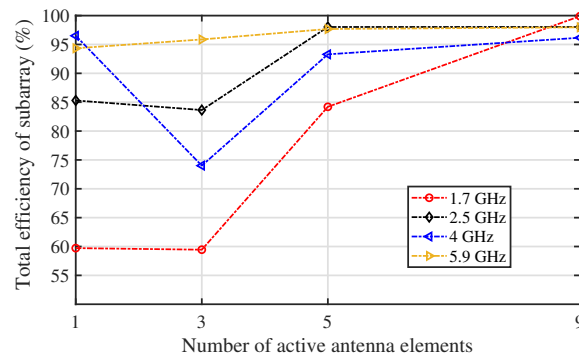
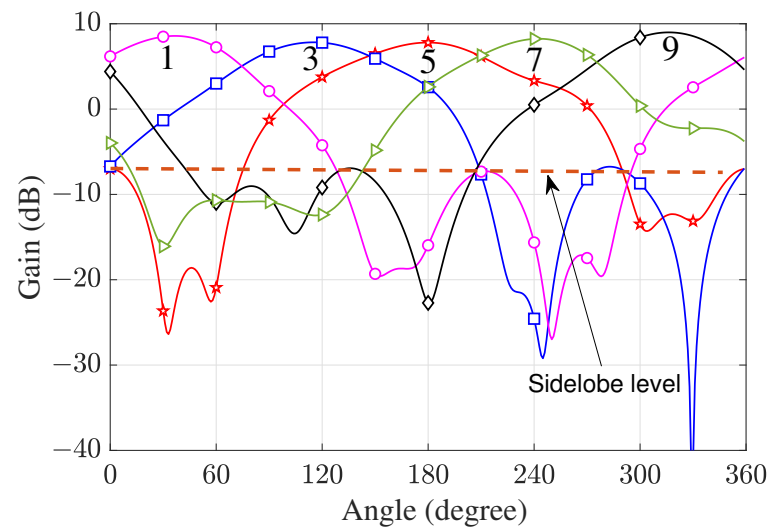


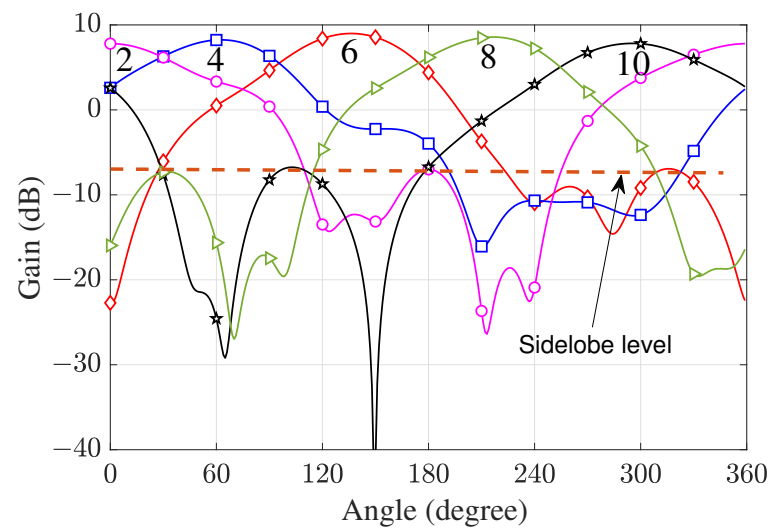
**Figure 8.** Total efficiency of the center element in the subarrays of different sizes, 1, 3, 5, and 9 elements in the subarrays, respectively. Far-field radiation patterns at 4 frequencies of 1.7 GHz, 2.5 GHz, 4 GHz, and 5.9 GHz were used for 4 different subarrays.

**Table 4.** Characteristics of the radiation patterns for subarrays of various sizes.

| Subarray Size<br>(Number of Elements) | XOY-Plane Beamwidth<br>(Degree) | YOZ-Plane Beamwidth<br>(Degree) | Gain<br>(dBi) |
|---------------------------------------|---------------------------------|---------------------------------|---------------|
| 1                                     | 51.6                            | 81.1                            | 7.81          |
| 3                                     | 48.6                            | 37.8                            | 7.16          |
| 5                                     | 68.3                            | 61.5                            | 8.80          |
| 9                                     | 33.6                            | 41.9                            | 10.54         |



(a)



(b)

**Figure 9.** The 10 independent beams formed in the horizontal plane of the cylindrical array; each beam was formed with a subarray of 9 elements, which are distributed evenly around the cylinder. (a) The 5 beams in the horizontal plane with an odd number. (b) The 5 beams in the horizontal plane with an even number.

The choice of a multibeam configuration was driven by the specific needs of the application, and this represents a trade-off between the complexity of the establishment and the benefits gained from it. From the four scenarios investigated, it appeared that, for subarrays formed by nine elements, 10 uniformly distributed subarrays can gather information from every direction in the horizontal plane. The relatively wide beamwidth

in the elevation plane can be made narrower with more elements becoming active in that direction, and accordingly, the gains of the beams can be improved. More beams can be formed by sharing array elements among subarrays to support more users in communication or satellite systems; however, the subarrays' configuration becomes more complicated as power splitters are needed.

#### 4. Results and Discussion

To demonstrate the performance of the cylindrical array in the presence of significant mutual coupling and its advantages for multibeam capability, a compact cylindrical array with a diameter of 50 mm was examined following the design illustrated in Figure 2. There were 80 dual-slant-polarized elements on the cylindrical surface. The height of the cylindrical array was 60 mm. The target operation frequency band ranged from 1.7 GHz to 6 GHz. The key aspects of the performance of the tightly coupled cylindrical array are compared with other existing array designs on convex surfaces in Table 5. The dual-slant-polarized cylindrical array based on tightly coupled crossed disks demonstrated a considerably wider bandwidth compared to other cylindrical arrays. The array investigated presented a higher mutual coupling between the adjacent elements, reaching as high as  $-9$  dB. Moreover, it has a compact structure, making it ideal for multibeam applications that also require a low-profile structure.

**Table 5.** Performance comparison of typical finite arrays on convex surfaces.

| Finite Array | Configuration         | Frequency Bandwidth | Maximum Coupling (dB) | Efficiency (%) | Subarray Size (mm)                |
|--------------|-----------------------|---------------------|-----------------------|----------------|-----------------------------------|
| [44]         | Spherical             | 8.7–11.2 GHz (25%)  | $-30$                 | NA             | 300 (diameter)                    |
| [45]         | Hemispherical         | 2.47 GHz            | $-35$                 | NA             | $268.8 \times 195.7 \times 30.48$ |
| [46]         | Soccer-like spherical | 1–2 GHz (67%)       | $-15$                 | NA             | $450 \times 450 \times 225$       |
| [47]         | Cylindrical           | 1.75–2.18 GHz (22%) | $-11$                 | NA             | $240 \times 100 \times 39$        |
| This work    | Cylindrical           | 1.7–5.9 GHz (110%)  | $-9$                  | 95             | $104 \times 104 \times 16$        |

The proposed cylindrical array yielded impedance matching over a frequency bandwidth of 110%. The broad impedance matching capability is related to the tight mutual coupling in the array. This is clearly indicated in Figures 5 and 6. When more elements are in the subarray and become active, the operation frequency bandwidth becomes wider. The subarray consisting of nine elements demonstrated the largest frequency bandwidth among the four subarray configurations. The active  $S_{11}$  of the center element is approximately below  $-15$  dB.

Providing multiple beams is an essential feature for antenna arrays to improve the scanning speed and increase the diversity gain. With a diameter of 50 mm, the proposed cylindrical array can produce 10 beams horizontally covering the entire horizontal plane by utilizing 10 subarrays with 80 elements of one polarization, and some of the elements were shared between neighboring subarrays. At the center frequency of 4 GHz, the gain varied between 7.81 dB and 10.54 dB, and 10 beams can be controlled to offer a fully agile coverage for the horizontal scan, and coverage of over  $40^\circ$  in the elevation domain was observed.

The efficiency of the array was investigated by monitoring the far-field radiation patterns under each subarray scenario at different frequencies. It was found that the improvement in efficiency due to the mutual coupling effect outweighed the concern about absorption-caused loss within the array. As illustrated in Table 3 and Figure 8, the total antenna efficiency of the center element significantly increased from approximately 60% to over 95% in most of the frequencies across the band. It was also noticed that, when the number of active elements increased, the total antenna efficiency rose, e.g., at 1.7 GHz, the total antenna efficiency changed from 59.72% for 1 active element to 99.9% with 9 elements becoming active together. It was noticed that the efficiency at the low frequency increased more rapidly as the number of active elements rose.

Mutual coupling can affect the impedance of individual array elements, and changes in impedance can lead to reflection and mismatch losses. Conventionally, one of the main concerns of mutual coupling is that it may decrease the overall efficiency of arrays. However, it was found from the cylindrical array that the enhanced mutual coupling had a positive effect, improving the efficiency instead of decreasing it, in particular at a low frequency.

It is worth mentioning that, despite high mutual coupling between the array elements in the proposed cylindrical array, the negative effect on the radiation patterns was found to be minimal, and smooth radiation patterns were obtained for subarrays of different configuration, as shown in Figure 7. No anomalies in the radiation patterns were observed from the low frequency of 1.7 GHz to the high frequency at 6 GHz; even the mutual coupling was more pronounced at the low-frequency band.

Arrays with multibeam capability can be beneficial to ITSs, particularly in the context of improving transportation efficiency and safety. Multibeam arrays could be used in sensor systems to improve the accuracy and coverage of data collection, as they can transmit and receive signals in multiple directions simultaneously, providing enhanced coverage and resolution compared to a single-beam system, e.g., 10 beams can be steered to produce a panorama view of the horizontal plane with a high resolution. The integration of multibeam arrays with ITSs would depend on specific use cases and technological advancements. These concepts represent the ongoing efforts to make transportation systems more efficient, safe, and technologically advanced.

## 5. Conclusions

The effect of mutual coupling in the CCA based on a tightly coupled disk antenna was investigated. It was revealed that enhanced mutual coupling was essential to obtain the ultra-wide bandwidth desired from such arrays. The efficiency of the subarray increased due to the mutual coupling as it contributed to improving the impedance matching. Hence, more energy was transported by the subarrays. A significant mutual coupling exists only between the elements that are physically close to each other, and this feature can be used to form multiple beams simultaneously spanning the entire azimuthal plane out of the cylindrical array. The array configuration shows a great prospect in ITS, where data from omnidirectional monitoring and a broader spectrum is required.

Multibeam cylindrical arrays are a versatile and powerful solution for applications that require simultaneous coverage of multiple directions. Their use is driven by the need for increased spectrum efficiency, adaptability, and improved performance in various applications such as RS, communication, and astronomy. The wideband operability of the examined cylindrical array in the presence of enhanced mutual coupling make it a more-effective option for these applications.

**Author Contributions:** Conceptualization, X.L. and Y.Z.; methodology, X.L.; validation, X.L.; formal analysis, X.L.; investigation, X.L.; resources, Y.Z. and H.L.; writing—original draft preparation, X.L.; visualization, Y.F.; writing—review and editing, Q.S., Y.F., H.L., Y.Z., A.E.-M. and M.T. All authors have read and agreed to the published version of the manuscript.

**Funding:** This work was supported in part by the National Natural Science Foundation of China under Grants 62174091 and 62201294, in part by the Post-Doc International Exchange Programme Y20210098, and in part by the Nantong Science and Technology Plan Project (No. MS22022093) and the Natural Science Foundation of The Jiangsu Higher Education Institutions of China (No. 23KJB580014).

**Data Availability Statement:** Data is contained within the article.

**Conflicts of Interest:** The authors declare no conflicts of interest.



## Abbreviations

The following acronyms are used in this manuscript:

|       |   |
|-------|---|
| AF    | Array factor                                |
| CCA   | Cylindrical conformal array                 |
| CPPAR | Cylindrical polarimetric phased array radar |
| EM    | Electromagnetics                            |
| EP    | Element pattern                             |
| GIS   | Geographic Information System               |
| ITS   | Intelligent transportation system           |
| OIR   | Optical–infrared                            |
| RS    | Remote sensing                              |

## References

- Zhu, J.; Wu, P.; Anumba, C.A. Semantics-Based Approach for Simplifying IFC Building Models to Facilitate the Use of BIM Models in GIS. *Remote Sens.* **2021**, *13*, 4727. [CrossRef]
- Ye, S.; Zhu, D.; Yao, X.; Zhang, N.; Fang, S.; Li, L. Development of a Highly Flexible Mobile GIS-Based System for Collecting Arable Land Quality Data. *IEEE J. Sel. Top. Appl. Earth Obs. Remote Sens.* **2014**, *7*, 4432–4441. [CrossRef]
- Earl, R.; Thomas, G.; Blackmore, B.S. The potential role of GIS in autonomous field operations. *Comput. Electron. Agric.* **2000**, *25*, 107–120. [CrossRef]
- Zhang, J.; Chen, L.; Wang, C.; Zhuo, L.; Tian, Q.; Liang, X. Road Recognition From Remote Sensing Imagery Using Incremental Learning. *IEEE Trans. Intell. Transp. Syst.* **2017**, *18*, 2993–3005. [CrossRef]
- Khechba, K.; Laamrani, A.; Dhiba, D.; Misbah, K.; Chehbouni, A. Monitoring and Analyzing Yield Gap in Africa through Soil Attribute Best Management Using Remote Sensing Approaches: A Review. *Remote Sens.* **2021**, *13*, 4602. [CrossRef]
- Kim, C.; Kim, S.; Jung, K. Adaptive Flow Control Using Movement Information in Mobile-Assisted Sensor Data Collection. *IEEE Sens. J.* **2020**, *20*, 12435–12446. [CrossRef]
- Yue, W.; Jiang, L.; Yang, X.; Gao, S.; Xie, Y.; Xu, T. Optical Design of a Common-Aperture Camera for Infrared Guided Polarization Imaging. *Remote Sens.* **2022**, *14*, 1620. [CrossRef]
- Ewan, L.; Al-Kaisy, A.; Veneziano, D. Remote Sensing of Weather and Road Surface Conditions: Is Technology Mature for Reliable Intelligent Transportation Systems Applications? *Transp. Res. Rec.* **2013**, 2329, 8–16. [CrossRef]
- Mondal, T.; Debnath, R.; Roy, J.S.; Bhadra Chaudhuri, S.R. Phased array antenna design for intelligent transport systems. In Proceedings of the 2009 IEEE International Workshop on Antenna Technology, Santa Monica, CA, USA, 2–4 March 2009; pp. 1–4. [CrossRef]
- Guntupalli, A.B.; Wu, K. Full-space scanning phased array system for future integrated high data rate communication over E-band and beyond. In Proceedings of the 2013 European Microwave Conference, Nuremberg, Germany, 9–11 October 2013; pp. 1607–1610. [CrossRef]
- Warnick, K.F.; Maaskant, R.; Ivashina, M.V.; Davidson, D.B.; Jeffs, B.D. *Phased Arrays for Radio Astronomy, Remote Sensing, and Satellite Communications*; Cambridge University Press: Cambridge, UK, 2018. [CrossRef]
- Paul, B.; Chiriyath, A.R.; Bliss, D.W. Survey of RF Communications and Sensing Convergence Research. *IEEE Access* **2017**, *5*, 252–270. [CrossRef]
- Tian, Y.; Liu, H.; Furukawa, T. Reliable Infrastructural Urban Traffic Monitoring via Lidar and Camer Fusion. *SAE Int. J. Passenger Cars-Electr. Electr. Syst.* **2017**, *10*, 173–180. [CrossRef]
- Zhu, Q.; Chen, L.; Li, Q.; Li, M.; Nüchter, A.; Wang, J. 3D LIDAR point cloud based intersection recognition for autonomous driving. In Proceedings of the 2012 IEEE Intelligent Vehicles Symposium, Madrid, Spain, 3–7 June 2012; pp. 456–461. [CrossRef]
- Barbagli, B.; Bencini, L.; Magrini, I.; Manes, G.; Manes, A.; Srl, N. A traffic monitoring and queue detection system based on an acoustic sensor network. *Int. J. Adv. Netw. Serv.* **2011**, *4*, 27–37. Available online: <http://www.iariajournals.org> (accessed on 11 August 2023).
- Seelan, S.K.; Laguetta, S.; Casady, G.M.; Seielstad, G.A. Remote sensing applications for precision agriculture: A learning community approach. *Remote Sens. Environ.* **2003**, *88*, 157–169. [CrossRef]
- Sanchez, G.H.; Saito, M.; Schultz, G.G.; Eggett, D.L. Use of High-Resolution Data to Evaluate the Accuracy of Mean and 85th Percentile Approach Speeds Collected By Microwave Sensors. In Proceedings of the Transportation Research Board 96th Annual Meeting (TRB), Washington, DC, USA, 8–12 January 2017; pp. 1–17. Available online: <https://trid.trb.org/view/1437310> (accessed on 1 September 2023).
- Karthikeyan, L.; Chawla, I.; Mishra Ashok, K. A review of remote sensing applications in agriculture for food security: Crop growth and yield, irrigation, and crop losses. *J. Hydrol.* **2020**, *586*, 124905. [CrossRef]
- Mao, X.; Tang, S.; Wang, J.; Li, X.Y. iLight: Device-free passive tracking using wireless sensor networks. *IEEE Sens. J.* **2013**, *13*, 3785–3792. [CrossRef]
- Golbon-Haghighi, M.-H.; Saeidi-Manesh, H.; Zhang, G.F.; Zhang, Y. Pattern Synthesis for the Cylindrical Polarimetric Phased Array Radar (CPPAR). *Prog. Electromagn. Res. M* **2018**, *66*, 87–98. [CrossRef]

21. Sishodia, R.P.; Ray, R.L.; Singh, S.K. Applications of Remote Sensing in Precision Agriculture: A Review. *Remote Sens.* **2020**, *12*, 3136. [CrossRef]
22. Odat, E.; Shamma, J.S.; Claudel, C. Vehicle Classification and Speed Estimation Using Combined Passive Infrared/Ultrasonic Sensors. *IEEE Trans. Intell. Transp. Syst.* **2018**, *19*, 1593–1606. [CrossRef]
23. Schoebel, J.; Buck, T.; Reimann, M.; Ulm, M.; Schneider, M.; Jourdain, A.; Carchon, G.J.; Tilmans, H.A.C. Design considerations and technology assessment of phased-array antenna systems with RF MEMS for automotive radar applications. *IEEE Trans. Microw. Theory Tech.* **2005**, *53*, 1968–1975. [CrossRef]
24. Agarwal, V.; Murali, N.V.; Chandramouli, C. A Cost-Effective Ultrasonic Sensor-Based Driver-Assistance System for Congested Traffic Conditions. *IEEE Trans. Intell. Transp. Syst.* **2009**, *10*, 486–498. [CrossRef]
25. Xu, J.; Hong, W.; Zhang, H.; Wang, G.; Yu, Y.; Jiang, Z.H. An Array Antenna for Both Long and Medium-Range 77 GHz Automotive Radar Applications. *IEEE Trans. Antennas Propag.* **2017**, *65*, 7207–7216. [CrossRef]
26. Zhu, B.; Sun, Y.; Zhao, J.; Zhang, S.; Zhang, P.; Song, D. Millimeter-Wave Radar in-the-Loop Testing for Intelligent Vehicles. *IEEE Trans. Intell. Transp. Syst.* **2022**, *23*, 11126–11136. [CrossRef]
27. Won, M.; Zhang, S.; Son, S.H. WiTraffic: Low-cost and non-intrusive traffic monitoring system using WiFi. In Proceedings of the 2017 26th International Conference on Computer Communication and Networks (ICCCN), Vancouver, BC, Canada, 31 July–3 August 2017; pp. 1–9.
28. Haferkamp, M.; Al-Askary, M.; Dorn, D.; Sliwa, B.; Habel, L.; Schreckenberger, M.; Wietfeld, C. Radio-based traffic flow detection and vehicle classification for future smart cities. In Proceedings of the 2017 IEEE 85th Vehicular Technology Conference (VTC Spring), Sydney, Australia, 4–7 June 2017; pp. 1–5.
29. Temiz, M.; Alsusa, E.; Danoon, L.; Zhang, Y. On the Impact of Antenna Array Geometry on Indoor Wideband Massive MIMO Networks. *IEEE Trans. Antennas Propag.* **2021**, *69*, 406–416. [CrossRef]
30. Fu, Y.; Zhang, Y.; Shi, Q.; Temiz, M.; El-Makadema, A.; Shi, J. A Foldable Tightly Coupled Crossed Rings Antenna Array of Ultrawide Bandwidth and Dual Polarization. *IEEE Access* **2022**, *10*, 86684–86695. [CrossRef]
31. Lv, X.; Zhang, Y.; Shi, Q.; Temiz, M.; El-Makadema, A. A Dual Slant-Polarized Cylindrical Array of Tightly Coupled Dipole Antennas. *IEEE Access* **2022**, *10*, 30858–30869. [CrossRef]
32. Liu, Y.; Yang, H.; Jin, Z.; Zhao, F.; Zhu, J. A Multibeam Cylindrically Conformal Slot Array Antenna Based on a Modified Rotman Lens. *IEEE Trans. Antennas Propag.* **2018**, *66*, 3441–3452. [CrossRef]
33. Li, Z.; Zhang, G.; Golbon-Haghighi, M.-H.; Saeidi-Manesh, H.; Herndon, M.; Pan, H. Initial Observations with Electronic and Mechanical Scans Using a Cylindrical Polarimetric Phased Array Radar. *IEEE Geosci. Remote Sens. Lett.* **2021**, *18*, 271–275. [CrossRef]
34. Redmond, K.; Meier, J.; Karimkashi, S.; McCord, M.; Meier, I.; Zhang, G.; Palmer, R.; Zahrai, A.; Schmidt, D.; Doviak, R.J.; et al. Cylindrical Polarimetric Phased Array Radar: Hardware design and mobile demonstrator. In Proceedings of the 2014 International Radar Conference, Lille, France, 13–17 October 2014. [CrossRef]
35. Sureau, J.-C.; Keeping, K. Sidelobe control in cylindrical arrays. *IEEE Trans. Antennas Propag.* **1982**, *30*, 1027–1031 [CrossRef]
36. Borgiotti, G.V.; Balzano, Q. Mutual coupling analysis of a conformal array of elements on a cylindrical surface. *IEEE Trans. Antennas Propag.* **1970**, *18*, 55–63. [CrossRef]
37. Borgiotti, G.V. Conformal Arrays, Ch. 11. In *The Handbook of Antenna Design*; Davies, D.E.N., Rudge, A.W., Eds.; Peter Peregrinus: London, UK, 1983; Volume 2.
38. Wang, Q.; He, Q.Q. An arbitrary conformal array pattern synthesis method that include mutual coupling and platform effects. *Prog. Electromagn. Res.* **2010**, *110*, 297–311. [CrossRef]
39. Kraus, J.D.; Marhefka, R.J. *Antennas for All Applications*; McGraw-Hill: New York, NY, USA, 2002.
40. Balanis, C.A. *Antenna Theory: Analysis and Design*; Wiley: Hoboken, NJ, USA, 2016.
41. Bird, T.S. *Mutual Coupling between Antennas*; Wiley: Hoboken, NJ, USA, 2021.
42. Erturk, V.B.; Rojas, R.G. Efficient Analysis of Input Impedance and Mutual Coupling of Microstrip Antennas Mounted on Large Coated Cylinders. *IEEE Trans. Antennas Propag.* **2003**, *51*, 739–749. [CrossRef]
43. Brown, A.D. (Ed.) *Electronically Scanned Arrays MATLAB® Modeling and Simulation*, 1st ed.; CRC Press: Boca Raton, FL, USA, 2012.
44. Knott, P. Design of A Triple Patch Antenna Element for Double Curved Conformal Antenna Arrays. In Proceedings of the 2006 First European Conference on Antennas and Propagation, Nice, France, 6–10 November 2006; pp. 1–4. [CrossRef]
45. Braaten, B.D.; Roy, S.; Irfanullah, I.; Nariyal, S.; Anagnostou, D.E. Phase-Compensated Conformal Antennas for Changing Spherical Surfaces. *IEEE Trans. Antennas Propag.* **2014**, *62*, 1880–1887. [CrossRef]
46. Geissler, M.; Woetzel, F.; Böttcher, M.; Korthoff, S.; Lauer, A.; Eube, M.; Wleklinski, M. Design and Test of An L-Band Phased Array for Maritime Satcom. In Proceedings of the 5th European Conference on Antennas and Propagation (EUCAP), Rome, Italy, 11–15 April 2011; pp. 2871–2875. Available online: <https://ieeexplore.ieee.org/> (accessed on 12 October 2023).
47. Quan, X.; Li, R.; Fan, Y.; Anagnostou, D.E. Analysis and Design of a 45° Slant-Polarized Omnidirectional Antenna. *IEEE Trans. Antennas Propag.* **2014**, *62*, 86–93. [CrossRef]

**Disclaimer/Publisher’s Note:** The statements, opinions and data contained in all publications are solely those of the individual author(s) and contributor(s) and not of MDPI and/or the editor(s). MDPI and/or the editor(s) disclaim responsibility for any injury to people or property resulting from any ideas, methods, instructions or products referred to in the content.